Reprinted from JOURNAL OF THE ATMOSPHERIC SCIENCES, Vol. 46, No. 13, 1 July 1989
American Meteorological Society



# The Marine Boundary Layer in the Vicinity of an Ocean Front

DAVID P. ROGERS

# The Marine Boundary Layer in the Vicinity of an Ocean Front*

DAVID P. ROGERS

*Scripps Institution of Oceanography, La Jolla, California*

(Manuscript received 25 October 1988, in final form 2 February 1989)

ABSTRACT

Aircraft observations obtained during the Frontal Air-Sea Interaction Experiment (FASINEX) are used to investigate the structure of the marine atmospheric boundary layer in the vicinity of an ocean front. A quasi-stationary sea surface temperature (SST) discontinuity of 2°C was maintained across the frontal zone throughout the duration of the experiment. The primary response of the atmosphere to changes in the SST was observed in the surface-related turbulence fluxes. In the case of warm air flowing over cold water, the boundary layer appears to develop an internal boundary layer (IBL) in response to the sudden change in the sea surface temperature. The organized updrafts and downdrafts within this layer collapse with entrainment–detrainment processes in these cells dominating the turbulence statistics. The IBL grows in response to the wind shear in this layer, although the surface shear stress is much smaller on the colder side of the front than on the warm. The depth of the IBL, and, in the absence of the IBL, the mixed layer are found to scale with the friction velocity and the Coriolis parameter.

The IBL confines the surface-related turbulent mixing and shear-driven processes to the lower layers of the atmosphere. Thus, the shallow boundary layer cloud field appears to be maintained primarily by radiative transfer within the cloud layer. Multiple cloud-capped mixed layers were frequently observed throughout the experiment. They appear to be directly related to the horizontal variation of the SST with deeper boundary layers and higher cloud levels formed over warmer water.

## 1. Introduction

The Joint Air–Sea Interaction (JASIN) experiment (Pollard 1978) revealed that the spatial variability of the sea surface temperature (SST) on a scale of 200 km or less gives rise to horizontal variability on similar scales in the atmosphere (Guymer et al. 1983). Observations have shown that the turbulent structure of the marine atmospheric boundary layer (MABL) has different scales on opposite sides of a SST discontinuity (Guymer et al. 1983). The processes which produce this ocean–atmosphere coupling are not well understood, but appear to be crucial for a complete understanding of the development of marine boundary layer clouds.

The importance of cloudiness as a climatic feedback mechanism has been recognized for a long time (Manabe and Wetherald 1967; Shukla and Sud 1981; and others). In particular, Schneider et al. (1978) investigated the feedback effects of global cloudiness on surface temperature; they highlighted the complexity of the problem by demonstrating that increases in the surface temperature could lead to both an increase and a decrease in cloud cover dependent on the large-scale dynamical structure. Ongoing observational and numerical modeling studies in extratropical latitudes have lead to the conclusion that surface temperature, boundary layer dynamics and thermodynamics, the structure of the free atmosphere, and cloud microphysics—all play an important role in determining fractional cloudiness (Rogers and Telford 1986; Rogers 1986; Charlson et al. 1987; and others). It is anticipated that continued effort in this area will lead to an improvement in the parameterization of boundary layer fractional cloudiness in general circulation models for both short-term weather prediction and climate studies.

Model results indicate that fractional cloudiness is determined by changes in the SST and advection of cool, dry air across the top of the MABL (Rogers 1986). The influx of a large amount of dryer, potentially warmer air due to entrainment instability through the top of the boundary layer results in the evaporation of the cloud layer from the base up. This leads to the accumulation of dryer, warmer air immediately below cloud base and the development of a temperature discontinuity between the cloud and subcloud layers (Deardorff 1980; Nicholls and Leighton 1986; Rogers 1986). The continued exchange between the cloud and subcloud layers, and subsequent cloud development depends strongly on the relative importance of the heat and moisture fluxes in the subcloud layer as well as cloud top mixing processes. Here we concentrate on

* FASINEX Contribution Number 69.

*Corresponding author address:* Dr. David P. Rogers, Scripps Institute of Oceanography, University of California, San Diego, La Jolla, CA 92093.

determining the structure of the subcloud boundary layer air and the implications for cloud development.

Numerical simulations of MABLs have shown that cloud-capped boundary layers are the preferred equilibrium solution in most cases (Kraus and Leslie 1982). In general, an increase in the SST is accompanied by an increase in the heat and moisture fluxes at the surface. If the inversion at cloud top is sufficiently strong, then the depth of a continuous cloud deck will be largely insensitive to changes of the SST. Alternatively, if the air above the inversion is cool and dry, the inversion may be sufficiently weak so that an enhancement of the surface fluxes will lead to marginal instability throughout the layer and the onset of entrainment instability (Mahrt and Paumier 1982; Businger and Shaw 1984). Although entrainment instability has been associated with the break up of stratus, it may have a negative feedback on turbulent mixing by causing a temperature discontinuity to develop at the top of the subcloud layer. Heat and moisture from the ocean will tend to remain in the subcloud layer with some transfer into the cloud layer through active convective elements. This was observed during the JASIN experiment by Nicholls et al. (1983), and it is a frequent feature of the tropical boundary layer (Nicholls and LeMone 1980). If the air–sea temperature difference remains large, complete overturning of the MABL may occur. It is not clear whether this leads to fractional cloudiness, or overcast conditions as the air temperature and humidity approach equilibrium with the underlying surface. The extent to which the cloud and subcloud layers are coupled is important for the development of the boundary layer (Nicholls 1984; Rogers 1986). The height of cloud base may vary considerably as a function of the exchange of air between the surface and the free atmosphere. The development of the entire MABL in the vicinity of an ocean front is likely to depend strongly on the variability of the turbulent structure. In addition, one would expect an ocean front to have a significant imprint on cloud cover through the entrainment process; in turn, changes in the radiation associated with the cloud layer will feed back to the SST. The air above the boundary layer and the orientation of the flow relative to the front are also very important. The cloud pattern will also depend on fields of convergence associated with any secondary circulation generated by the front (Businger and Shaw 1984).

This paper discusses the response of the MABL to sudden changes in the SST. Data were obtained from the Frontal Air–Sea Interaction Experiment (FASINEX) in which the response of the ocean and the atmosphere to a weak oceanic temperature front was observed (Stage and Weller 1985, 1986). Satellite data from the FASINEX area have been analyzed on a monthly time scale by Gautier and Bates (1988). They observed that the thermal front acted to reduce the cloud cover on the warmer side, concluding that thinner, more highly broken clouds occurred over the warm water whereas thicker, more homogeneous clouds are found over the cold side. However, on synoptic and smaller temporal and spatial scales the effect of the SST is less clear. Thus it is important to determine the extent to which the local SST determines the overlying cloud field and the sensitivity of marine cloudiness to changes in the SST.

## 2. Frontal Air–Sea Interaction Experiment (FASINEX)

The background, objectives and the scientific plans for FASINEX have been described by Stage and Weller (1985, 1986) and the aircraft measurement program has been discussed in detail by Friehe and Williams (1988). The experimental region was located between 28° and 29°N, 69° and 71°W, roughly southwest of Bermuda. Aircraft were deployed from Raleigh, North Carolina; Wallops Island, Virginia; Miami, Florida; and Bermuda (Fig. 1).

Six aircraft, two ships and a moored array of buoys were used in the experiment. Three of the aircraft made detailed meteorological and turbulence measurements, one collected microwave scatterometer data, one made large scale ocean wave measurements, and one made LIDAR measurements of the inversion/cloud height. The primary source of data for the work discussed here was the NCAR Electra aircraft which made detailed meteorological and turbulence measurements. The NCAR Electra, in conjunction with other aircraft, flew a box pattern centered on the ocean thermal front at an altitude of 30 m (Fig. 1, insert). This pattern was designed to measure the wind field, divergence and curl. The box was oriented so that the front generally bi-

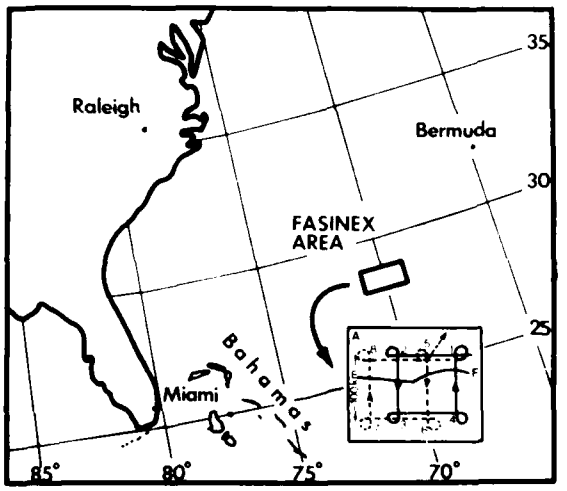


FIG. 1. Map showing the location of the FASINEX area. Aircraft were deployed from Raleigh, NC; Wallops Island, VA; Miami, FL and Bermuda. Insert A is a schematic of the turbulence aircraft flight pattern in the vicinity of the front (denoted by F).

sected the north–south legs; each leg was about 100 km in length. Vertical profiles of the thermodynamic structure and wind field were obtained from aircraft descents on the north side and ascents on the south side of the front. These were obtained at the beginning and end of each observation period on station at the front. On station, flights were dedicated to measuring the horizontal variability of the turbulent structure of the air at multiple levels across the front. The horizontal legs flown at 30 m are used to investigate interactions between the surface fluxes and the development of clouds over the experimental area. A description of the NCAR Electra instrumentation and accuracy can be found in Lenschow (1986).

The NCAR Electra flew six missions in the FASINEX study area between 16 and 24 February 1986 (Julian days 47–55). Three days, 48, 49 and 52, were selected for this study. Each of these is representative of a distinct surface wind regime. On day 48 the wind was from the east, blowing parallel to the front within the box pattern. On day 49 the air flowed from the south from over the warmer to the cooler water, while on day 52 the wind reversed direction blowing from over the cooler water to the warmer water (Table 1).

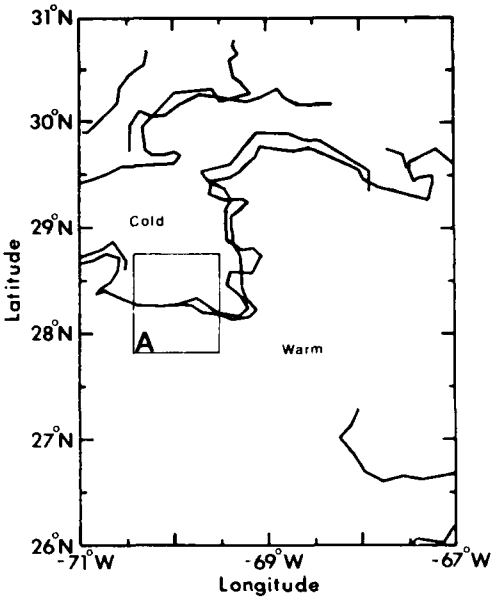


FIG. 2. Digitized frontal region for day 48 from the AVHRR image (after Halliwell et al. 1987). The insert A represented the position of the FASINEX aircraft study area.

## 3. The SST distribution and cloud fields

The main frontal location has been digitized from the NOAA-9 Advanced very high resolution radiometer (AVHRR) data for the entire FASINEX period by Halliwell et al. (1987). The Box pattern was centered on the east–west surface expression of the front; however, warm tongues of water extended northward to the east and west of the FASINEX region (Fig. 2). This pattern is representative of the SST field on day 48; the surface was obscured by clouds on the other two days. The front was distinguished by as much as 2°C temperature difference in the region of the strongest gradients. The surface temperatures typically varied from about 17° to 22°C in the FASINEX area. Towards the end of the experimental period the warm water to the west of the FASINEX box intruded into the box with considerable structure (Pollard 1986). The satellite image revealed that on day 48 a few scattered cumulus clouds appeared to be confined to the boundary layer over the warmer water in the southern part of the box. These clouds were generally banded and organized in an east–west direction parallel to the surface wind. Deeper, more horizontally uniform sheets of clouds, with tops near 0°C, were observed at the eastern and western extremities of the region over the northward extension of the warmer water. In contrast, on day 49 altostratus type clouds, with cloud top temperatures below −40°C, covered the entire FASINEX region obscuring the boundary layer clouds. On day 52 the FASINEX region was covered partially by low level bands of cloud which were parallel to the surface wind and similar in structure to those observed on day 48; however, in this case they were observed over the entire region (Table 1).

TABLE 1. Summary of flights.

| Flight day | Surface wind direction | Comments |
|---|---|---|
| 48 | East | Parallel to east–west expression of the front and perpendicular to north–south expression |
| 49 | South | Wind blowing from the warm to the cold water |
| 52 | North | Wind blowing from the cold to the warm water |

The distribution of the aircraft measured SST for day 48 is shown in Fig. 3a. The front was sharp and oriented in an east–west direction with the warmer water to the south. Outside of the immediate frontal region the SST was relatively uniform except in the northeast corner of the box where there was an east–west temperature gradient. The latter reflects the proximity of the warmer water to the east of the FASINEX region observed in Fig. 2. The frontal region was between 5 and 10 km wide with a SST increase of about 2°C across the front from about 19.8°C on the cooler side. On the warm side of the front the SST increased gradually to a maximum temperature about 25 km away from the interface. On the cold side of the front the SST was relatively constant. The mean surface winds, within the FASINEX area, were easterly, parallel with

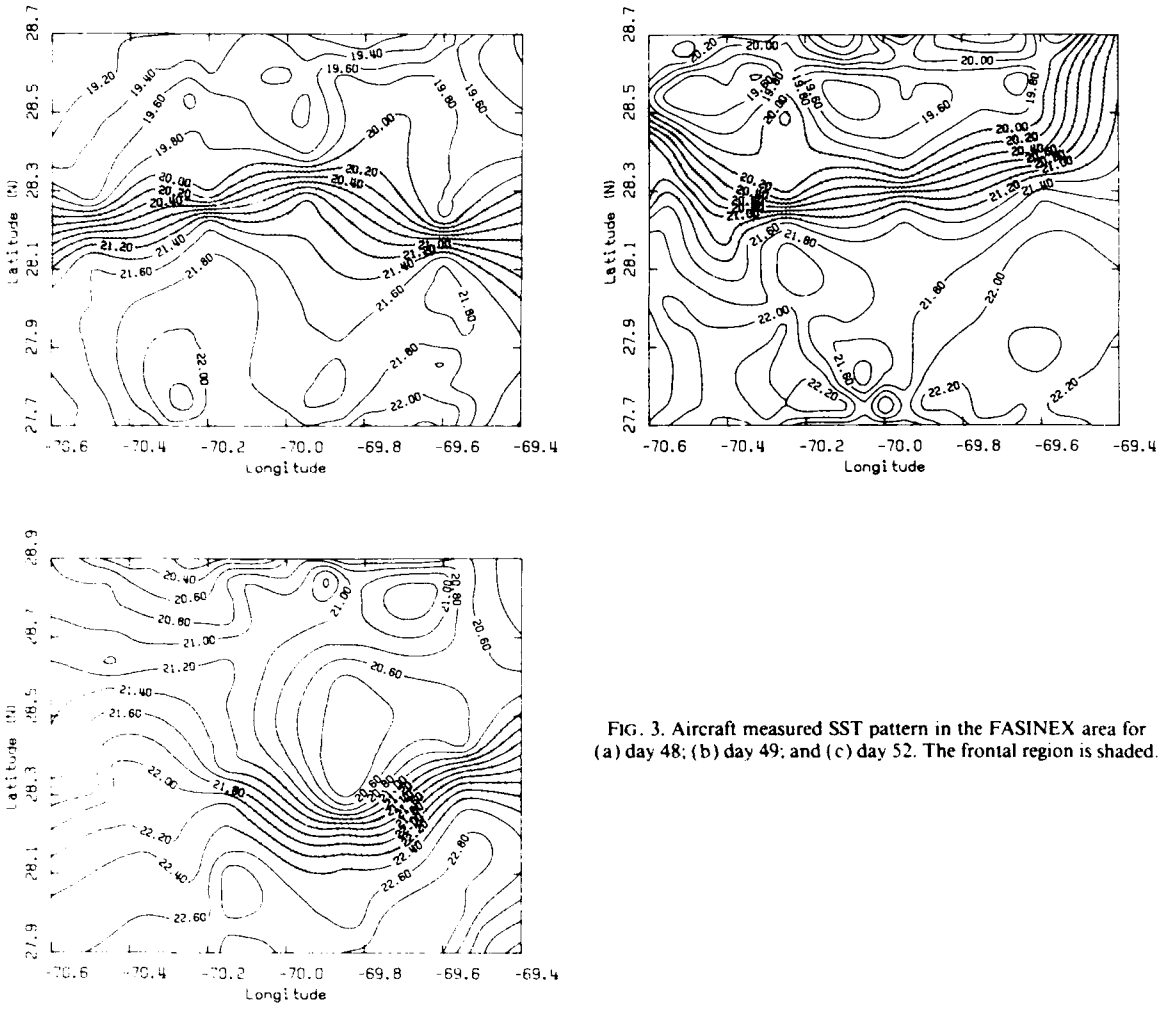


FIG. 3. Aircraft measured SST pattern in the FASINEX area for (a) day 48; (b) day 49; and (c) day 52. The frontal region is shaded.

the front. The same feature was clearly discernible on day 49; however, warmer water began to move northward at the eastern and western edges of the FASINEX area (Fig. 3b). By day 52, the frontal structure had weakened. Although there was still a strong north to south temperature gradient, the well-defined temperature structure observed on the previous days had begun to break down (Fig. 3c).

## 4. Vertical structure of the boundary layer

Profiles were obtained during the aircraft descent to the north of the FASINEX area generally over the cooler water and during ascent over warmer water to the south of the area. In addition, the NOAA-P3 aircraft flew stack patterns at the northern and southern extremities of the box. The latter were reported on by Khalsa and Greenhut (1988).

Five distinct layers were discernible on the cold side of the front on day 48: an internal boundary layer (IBL) or surface layer; a mixed layer which extended from about 300 to about 1100 m; a transition layer between about 1100 and 1500 m in which the potential temperature, $\theta$, increased with height; a cloud layer which was located between 1500 and 1800 m; and an inversion layer which was less than 50 m deep (Fig. 4a). The IBL has been previously observed intermittently in a study of marine stratiform clouds (Nicholls and Leighton 1986). These authors referred to the layer as a surface or Ekman layer representing the limit of the surface generated turbulence mixing. The transition layer was similar to that observed in the tropics (Nicholls and LeMone 1980). $\theta$ increased by about 0.5 K from the top of the mixed layer to cloud base, suppressing dry turbulent mixing originating lower in the MABL. Immediately above cloud top $\theta$ increased by 5 K forming a moderate temperature inversion. The variability in the inversion was due, primarily, to hor-

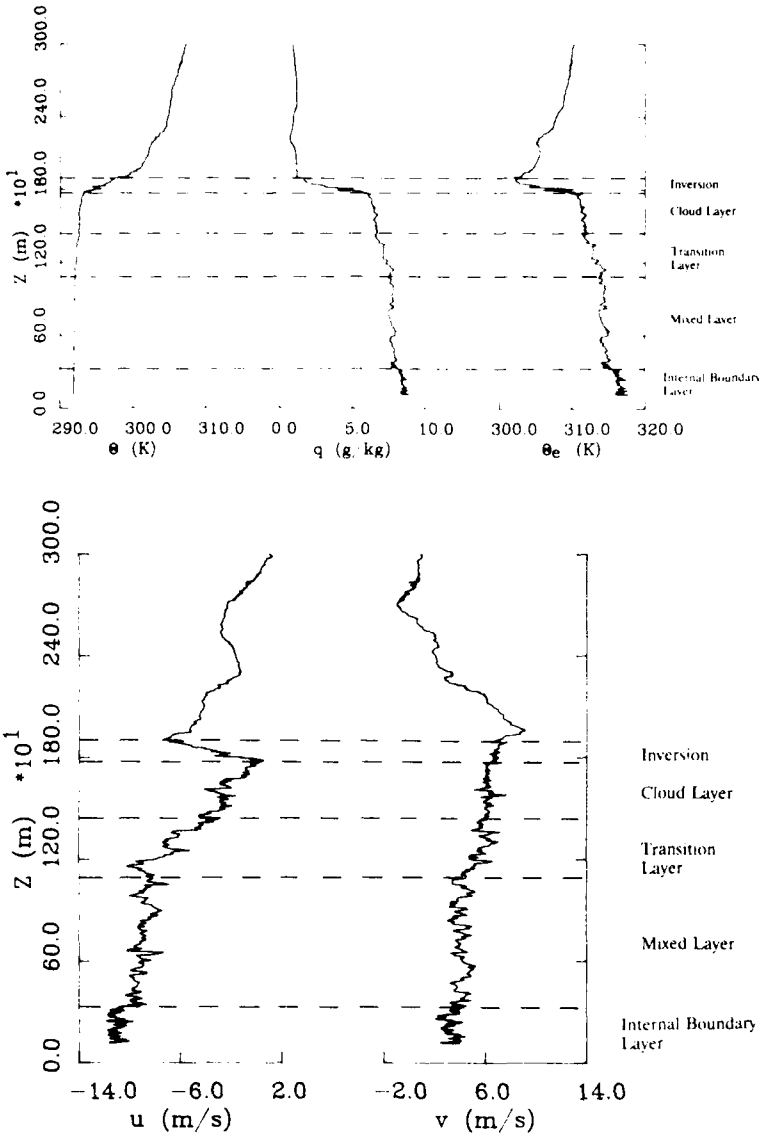


FIG. 4. (a) Vertical profiles of $\theta$, $q$ and $\theta_e$ obtained during the descent sounding over the cold water on the north side of the front on day 48. The MABL is divided into five layers: 1) internal boundary layer; 2) mixed layer; 3) transition layer; 4) cloud layer; and 5) inversion layer. (b) Vertical profiles of the horizontal wind components obtained during the descent sounding over the colder water on the north side of the front on day 48.

izontal changes in the inversion height along the flight path. Cloud base height also varied considerably. This profile was obtained near the northeast corner of the FASINEX area close to the warmer water located to the east of the region (Fig. 2). Thus, much of the air in the boundary layer most likely originated over the warmer water. The high moisture content of the marine boundary layer is observed in the mixing ratio, $q$, profile which dominated the equivalent potential temperature ($\theta_e$). Within the mixed layer $q$ was about 7.8 g kg$^{-1}$; however, below 300 m in the IBL, the moisture content was much higher resulting in a maximum in $\theta_e$. The top of this layer appears to have been the maximum extent of the surface-related turbulent mixing. This layer appears to have been decoupled from the mixed layer and may represent the development of an internal boundary which formed as the air flowed from the warm water to cold water. There is a discontinuity in $q$ and, hence, in $\theta_e$ at the top of the IBL. In contrast $\theta$ is continuous throughout the subcloud layer with no

discontinuity between the top of the IBL and base of the mixed layer. Elsewhere, turbulent mixing appears to have been quite weak. The estimated lifting condensation level (LCL) for air originating in the mixed layer was above the top of the IBL and, therefore, above the level reached by surface-related turbulent mixing. Through the transition layer, separating the cloud and subcloud layers, $q$ decreased rapidly. This decrease continued more slowly within the cloud layer where the lapse rate was close to the saturation adiabat. Across the inversion $q$ decreased by about 5 g kg$^{-1}$ resulting in a decrease of $\theta_e$ to a minimum immediately above the MABL. This feature is frequently observed at the top of the MABL. Betts and Albrecht (1987) explained the phenomenon in terms of radiative cooling in the air subsiding above the boundary layer. Within the free atmosphere $\theta_e$ increased in height in response to the increase in $\theta$ and the low mixing ratio. The $\theta_e$ discontinuity of 9 K across the inversion exceeded the critical entrainment instability value so that the cloud field was controlled, at least partially, by entrainment.

Below about 1100 m the air flow was primarily from the east, veering to the south above the mixed layer up to the base of the inversion (Fig. 4b). The strongest shear occurred in the $u$ component at cloud base and cloud top. Shear was also supported at about 300 m elevation, corresponding with the top of the IBL.

An important feature of the boundary layer on the warm side of the front was the presence of a multiple boundary layer structure. The most prominent structures in the boundary layer were two well-mixed layers and two cloud layers (Fig. 5a). The surface based mixed layer extended up to about 800 m. Scattered cumulus clouds occupied a layer between about 800 and 1300 m (layer A). Above this was a deep inversion layer extending up to the base of an elevated mixed layer located between about 1900 and 2600 m. Scattered clouds occupied the upper 300 m of this layer (layer B). A comparison of the profiles of $\theta$ from over warmer water and over the colder water reveals that the free atmosphere had a similar temperature profile in both cases above 2600 m; thus the variability in the structure was confined to the MABL. Here the average temperature of the profile from the colder side of the front was about 1.2 K lower than over the warmer water. The mixing ratio was also larger on the warmer side of the front, and remained high up to the base of the inversion; $q$ dropped rapidly to about 0.5 g kg$^{-1}$ in the free atmosphere. The high moisture content in the upper part of the MABL resulted in maximum values of $\theta_e$ in the elevated mixed layer. Throughout this layer there is considerable variability in the moisture content. Although these data have been averaged to 1 Hz, the fluctuations in the horizontal wind components (Fig. 5b) and the thermodynamic structure indicate that turbulent mixing extended below the cloud field into the subcloud layers. The high level of turbulence throughout the surface based mixed layer and lower cloud layer, despite a stable transition layer below cloud base which limits the vertical exchange of buoyancy and momentum, suggests that there was more than one source of turbulent kinetic energy. Thus mixing within the cloud layer was most likely maintained by radiative processes rather than surface-related turbulence mixing. The layer separating the two major MABL structures was strongly stratified, but only weakly turbulent.

The origin of the air in the boundary layer can be investigated using a mixing diagram approach. Several methods have been proposed, for example, Paluch (1979) and Betts (1982). These extend the concept of quasi-conservative mixing originally introduced by Taylor (1917). Here we use the method developed by Paluch (1979) and applied by Gardiner and Rogers (1987) to the evolution of continental cumulus clouds. Two conservative thermodynamic variables are defined: the total mixing ratio, $Q$, and the wet equivalent potential temperature, $\theta_q$. The latter is a measure of the specific entropy and is conserved along a reversible wet adiabat. In general, a mixture of air from two levels will lie on a straight line connecting the two points with mixing proportions varying along the line.

The mixing diagram for the day 48 colder water profile is shown in Fig. 6a. In addition to the profile data, the $\theta_q$–$Q$ values for several SSTs representative of temperatures on each side of the front are also shown. Air in equilibrium with the underlying surface will be close to the "saturation" line connecting these points. Mixing line $x$ indicates that the air below 300 m had been modified by the underlying cooler water (SST $\approx$ 19°C). Air higher up in the MABL mixed along line $y$, combining air originating over warmer water and air from the top of the MABL. The air between these mixing lines indicates that some mixing occurred between the surface layer and the overlying air. This region contains most of the in-cloud points which suggests that the cloud layer had partially mixed with air from below cloud base. This corresponds with the transition layer observed in the vertical profiles. Most of the in-cloud data indicate that mixing occurred only with air in the immediate vicinity of the cloud field. However, the in-cloud points marked C in Fig. 6a, are an exception; these represent mixtures of air from the surface and above the inversion. Unfortunately, the sparsity of the data prevents a specific determination of the origin of this cloudy air and the possibility of instrumental wetting problems cannot be excluded.

The mixing diagram for the day 48 sounding over the warmer water is shown in Fig. 6b. Two distinct mixing lines are apparent: from the surface to about 1300 m (line $x$) and from about 1800 to 2600 m (line $y$). These regions were separated by a dry layer where $\theta_e$ was a minimum. The air in the lower mixed layer was a mixture of air from two sources; the ocean surface in the vicinity of 20°C water and the region immediately below the dry layer (line $x$). These mixtures con-

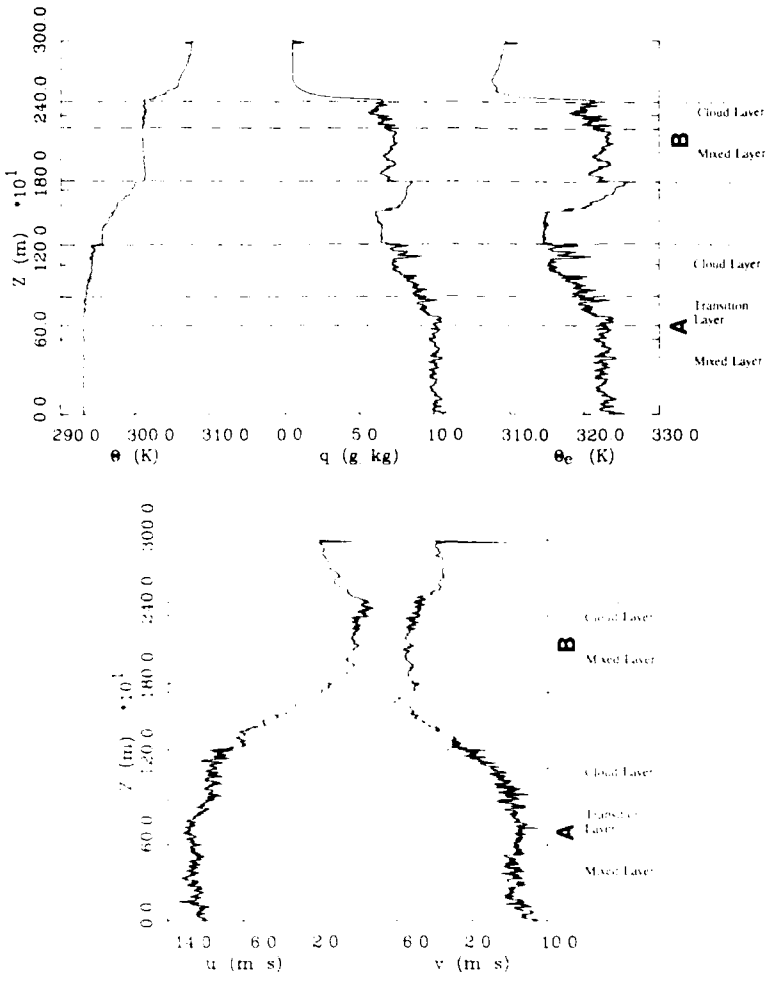


FIG. 5. (a) Vertical profiles of $\theta$, $q$ and $\theta_e$ for the air mass originating over the warmer water on the south side of the front on day 48. Two distinct boundary layer structures, denoted A and B, are identified. Layer A consists of a mixed layer, transition layer and cloud layer. Layer B consists of a mixed layer and a cloud layer. (b) Vertical profiles of the horizontal wind components for the air mass originating over the warmer water on the south side of the front on day 48.

tained about 30% surface air and 70% air which originated near the top of layer A (Fig 5a). The in-cloud parcels in this layer consisted entirely of mixtures of air from within the mixed layer; mixing across the dry region (1300–1800 m) was negligible. These results may be contrasted with the continental convective cloud observations of Gardiner and Rogers (1987), in which air from great heights was mixed down towards cloud base. In contrast, layer B consisted of a mixture of air from the base of the MABL inversion and air originally in the vicinity of approximately 24.5°C water (line $\gamma$). Such warm water was not fount in the FASINEX region. The dryness of the air between layers A and B is characteristic of the free atmosphere. Thus the elevated layer appears to have been an anomalous feature of the MABL. Since the wind in this layer was from the northwest, this air was probably advected into the FASINEX region from the cloud field to the west of the area shown in Fig. 2.

On day 49 the temperature inversion capping the marine layer was much weaker (Fig. 7a). In this case the wind direction was from the south from over the warmer water to the colder water. Deep convective clouds were present throughout the latter part of the flight with multiple cloud bases and tops, and occasional precipitation. In this case, the profiles obtained on each side of the front were quite similar. The mixed layer extended up to about 700 m above an IBL that

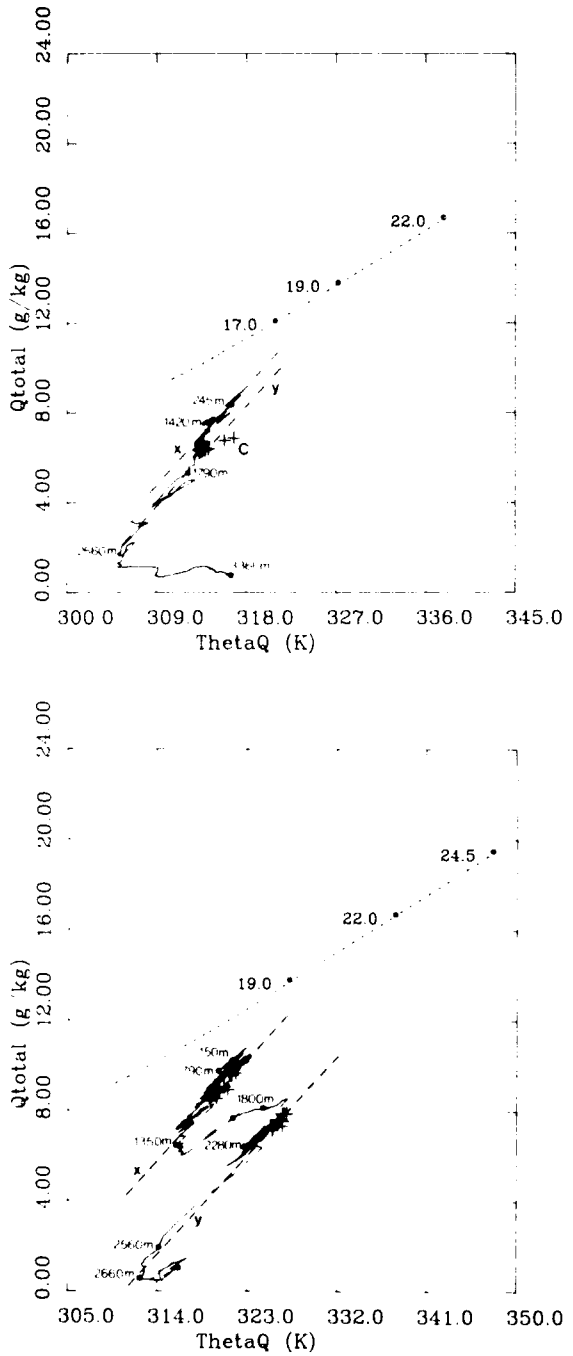


FIG. 6. (a) Mixing diagram for the descent profile over the colder water on day 48. $Q_{total}$ represents $Q$ and Theta$Q$ represents $\theta_q$. The points marked 17, 19 and 22 represent the $Q - \theta_q$ positions for saturated air at these respective SSTs. A saturation curve connects these points. Two mixing lines $x$ and $y$ are identified. In-cloud values are denoted by crosses (+). The points marked C represent the highest cloud level within the boundary layer. (b) Mixing diagram for the ascent profile over the warmer water on day 48.

was between 200 and 300 m deep on the cooler side of the front. There is some uncertainty in the depth of this layer because of variations in aircraft positions. The top of the surface layer was capped by a very shallow, sheared region (Fig. 7b). This is similar to the structure observed over the cooler water on day 48 with the wind direction from the east, apparently, also downwind of a warm water source. On the warm side of the front the mixed layer extended from the surface to about 600 m (Fig. 8). The top of the mixed layer, on both sides of the front, was distinguished by a large discontinuity in the mixing ratio and, consequently, the equivalent potential temperature. Overall, $\theta$ was approximately 2 K warmer up to 1800 m and $q$ approximately 4 g kg$^{-1}$ higher below the top of the mixed layer than observed on day 48. In contrast to the previous day, the $q$ profiles indicate that there was considerable interleaving of moist and dry layers throughout the lower atmosphere. In some of these layers $q$ and $\theta_e$ were nearly constant. A shallow cloud layer, about 100 m deep, was encountered at the top of the mixed layer on the cold side of the front; however, the cloud field was not penetrated during the ascent sounding below 5000 m.

Turbulence was much weaker than previously observed and confined, almost exclusively, to the mixed layer. Figure 7b suggests that, on the cold side of the front, the turbulence activity was less in the IBL than in the mixed layer. This would be expected since the air temperature exceeded the surface temperature and thus the IBL was quite stable (see section 5). Furthermore, both layers on the cold side indicated lower turbulence intensities than on the warm side of the front. Below the top of the mixed layer, on both sides of the front, the air was primarily from the south. On the cold side of the front, there was a region of strong shear from the top of the mixed layer to about 1500 m. Above this region the airflow was from about 250° with considerable small scale variability in the structure. The discontinuity in humidity at the top of the mixed layer on the warm side of the front was much less pronounced than that observed over the colder water. However, strong shear was also observed from the top of the mixed layer to about 1500 m. Above this, the flow was from about 230°.

The mixing diagram for the warm and cold water profiles on day 49 indicates that there was considerable continuity in the structure of the lower atmosphere across the front (Fig. 9). Over the warmer water the air below approximately 1000 m consisted of mixtures of air originating near the surface, in the vicinity of 22°C water, and this level. The mixed layer contained approximately 80% air originating at the surface. An intrusion of upper level moisture was similar in structure to that observed over the warm side of the front on day 48. Once again this air appears to have originated in the vicinity of 24.5°C water. As the boundary

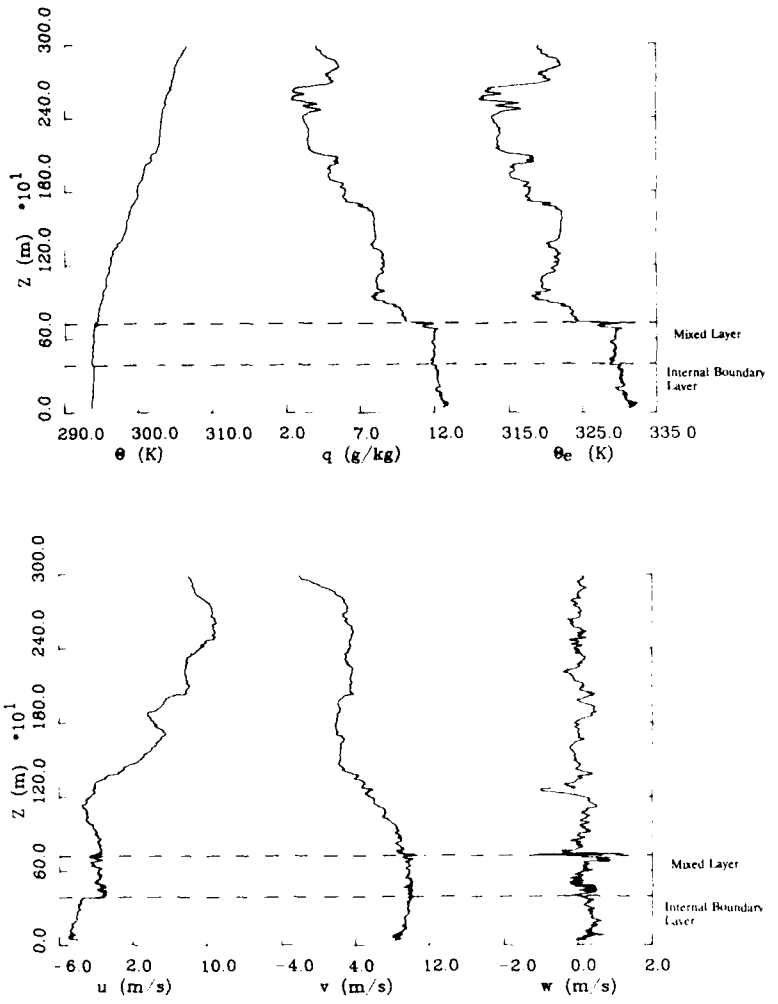


FIG. 7. (a) Vertical profiles of $\theta$, $q$ and $\theta_e$ for the air mass originating over the colder water on the north side of the front on day 49. The depth of the entire MABL is not clearly identified. The boundary layer consists of two layers: a well developed internal boundary layer and a mixed layer. Clouds occupy the upper portion of the mixed layer which is capped by a discontinuity in humidity. (b) Vertical profiles of the horizontal and vertical wind components from the descent sounding over the colder water.

layer passed over the cooler water, the surface-driven turbulence was confined to the IBL. Therefore, turbulent mixing within the mixed layer was probably maintained by radiative transfer within the cloud at the top of this layer. The mixed layer was composed of a mixture of about 50% air originated near the ocean surface in the vicinity of 22°C and 50% air originating at about 1100 m. Thus, as indicated by mixing line $y$ in Fig. 9, the boundary layer air on both sides of the front had a similar origin. Continuity is therefore preserved over approximately 250 km. In view of the development of a surface layer over the cold water, it is difficult to explain the differences in the temperature and humidity of the mixed layer air in terms of surface-related mixing processes. The lower $\theta_q$ and $Q$ values in the mixed layer, over the cold water, appear to be due to mixing with cooler, dryer air aloft. The region between 1000 and 2400 m was anomalously dryer, and cooler on the cold side of the front compared with the observations over the warmer water. Entrainment of this air into the top of the mixed layer would result in the cooling and drying out of the boundary layer down, at least, to the top of the surface layer. The sharpness of the mixing ratio profile, over the cloud water (Fig. 7a) is indicative of cloud top entrainment activity. Above 2400 m, the profiles are very similar on both sides of the front.

On day 52 there was a more pronounced multiple

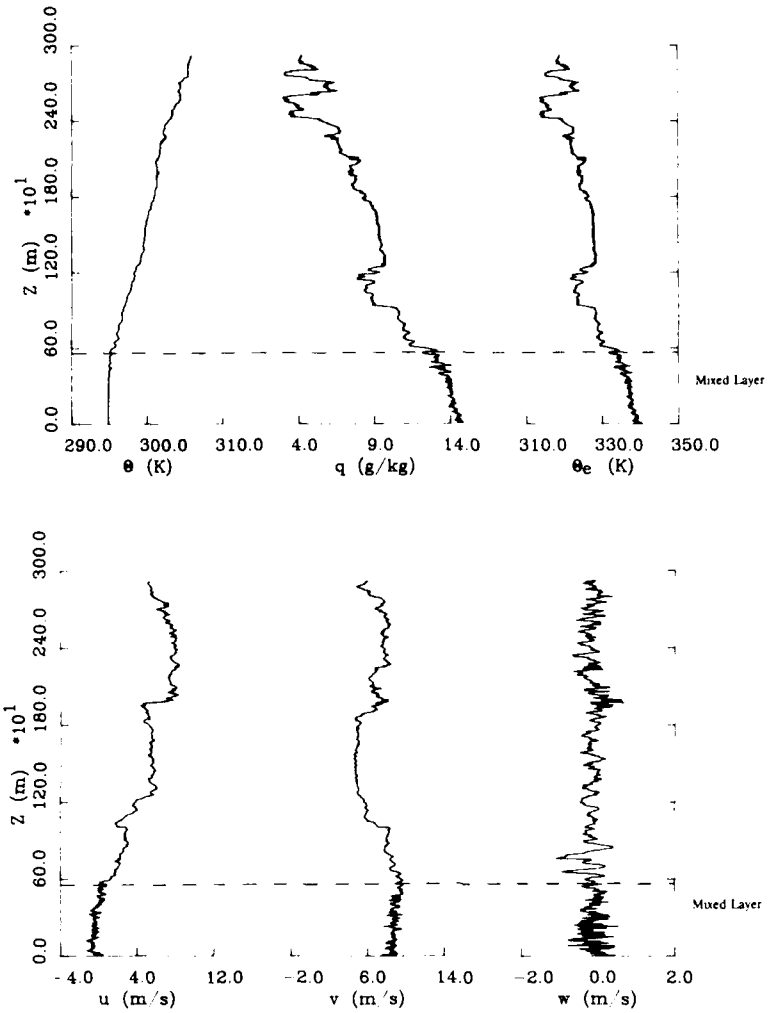


FIG. 8. (a) Vertical profiles of $\theta$, $q$ and $\theta_e$ obtained during the ascent sounding originating over the warmer water to the south of the front on day 49. A single mixed layer, extending down to the sea surface is identified. (b) Vertical profiles of the horizontal and vertical wind components obtained during the ascent sounding over the warmer water on day 49.

boundary layer structure similar to that observed over the warm water on day 48. However, in contrast to both days 48 and 49, this structure is observed primarily in the temperature profile since the mixing ratio in the upper layer was only about 25% of its near surface value (Fig. 10). Both profiles were obtained on the cold side of the front. The surface based boundary layer extended up to about 1200 m (layer C). There was a very shallow surface layer confined to the lower 100 m of the atmosphere; a mixed layer which extended from the top of this layer to about 700 m; and a layer of scattered cumulus clouds which extended up to approximately 1000 m. The elevated mixed layer occupied a layer from about 1500 to 2200 m capped by a deep potential temperature inversion extending up to about 2800 m (layer D). No clouds were penetrated in this layer, although scattered clouds were observed at this altitude. The ascent profile was obtained about three hours later to the northwest of the Box, the structure was almost identical, except for warming of the MABL, possibly due to subsidence which had strengthened the capping inversion.

The mixing diagram clearly indicate that these profiles were almost identical with the layer C mixed layer air originating over 19°C water (Fig. 11). The mixed layers identified in layer D appear to have originated over a warmer ocean surface; however, the very low mixing ratios indicate that this air had mixed extensively with the surrounding environment, as observed on day 49.

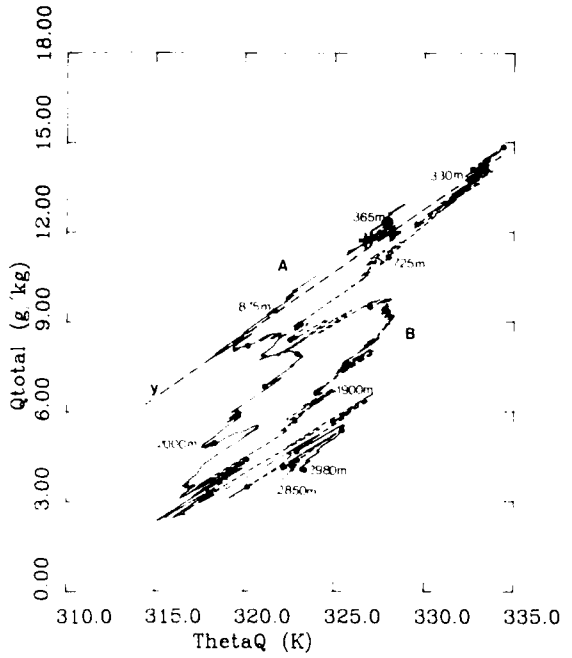


FIG. 9. Mixing diagram for the cold water sounding (A, solid line) and the warm water sounding (B, dashed line) soundings on day 49. The mixing line y connects the air in the mixed layers on both sides of the front.

## 5. Mean horizontal structure

The mean horizontal structure of the FASINEX boundary layer was obtained from the NCAR Electra and NRL-P3. The Electra measurements were obtained at 30 m nominal altitude. Time series of $\theta$, $q$, cloud base temperatures (TCB), SST, sea–air virtual potential temperature difference ($\Delta\theta_v$) and the LCL for two crossings of the front on day 48 are shown in Fig. 12. These legs differed only in so far as there was a slightly lower overall SST (about 0.5°C) and lower values of $q$ (0.5–1.0 g kg$^{-1}$) on leg 5-6 compared with leg 2-3 (Fig. 1). This resulted in a lower sea–air temperature difference and higher lifting condensation levels on leg 5-6. On both legs, clouds were observed only over the warmer water. The LCL varied from a maximum of about 950 m on the warm side to a minimum of about 800 m on the cold side of the front. Considerable fluctuations occurred throughout the time series primarily due to fluctuations in humidity and the overall gradient in temperature across the front. The estimated LCL from the vertical profiles corresponded with cloud base on the warmer side of the front, but was considerably lower than the observed cloud base on the cold side of the front. However, as discussed above, the LCL was above the level reached by surface-related turbulence mixing which was confined to the IBL on the cold side of the front.

Along both of the legs $q$ remained relatively constant although there was a sharp gradient in $\theta$ across the front. On leg 2-3 the gradient in $\theta$ is displaced over the cooler water, whereas, on leg 5-6 the change in $\theta$ coincided more nearly with the strongest temperature gradients in the ocean. On leg 2-3, estimates of $\Delta\theta_v$ along these flight tracks indicate that the minimum sea–air temperature difference occurred over the colder water, immediately to the north of the strongest ocean gradient. These displacements clearly indicate that there was cross frontal flow from the warmer water to the colder water, although the source of this air may have been to the east of the area. The decrease in the variability of $\theta$ from the warm to the cold side of the

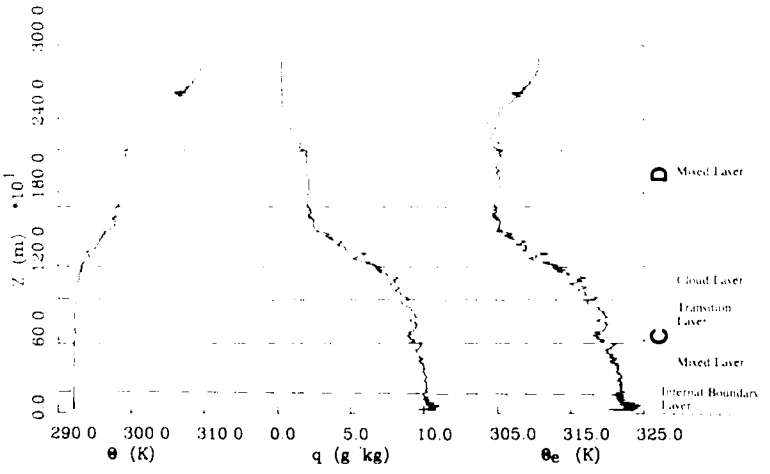


FIG. 10. Vertical profiles of $\theta$, $q$ and $\theta_e$ obtained during the descent sounding on the colder side of the front on day 52. The boundary layer structure is similar to that observed on day 48 (Fig. 4b).

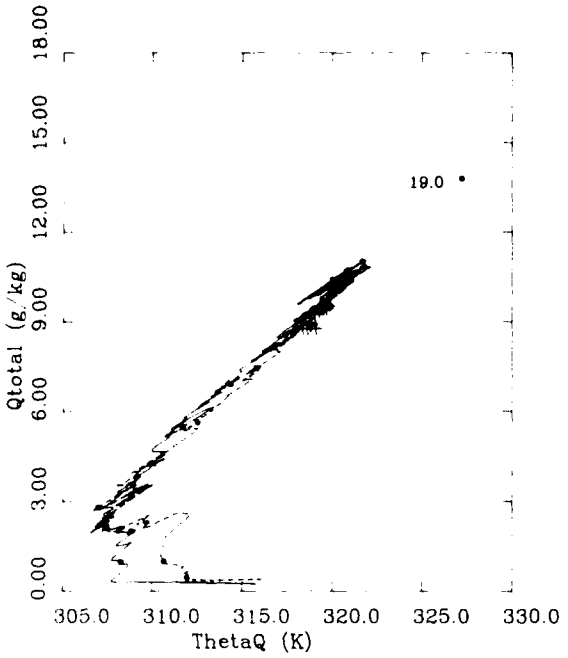


FIG. 11. Mixing diagram for the cold water sounding (solid line) and the warm water sounding (dashed line) profiles on day 52. Both profiles were obtained over the colder water.

front is indicative of a significant change in the convective scales on each side of the front.

Time series of $\theta$, $q$, TCB, SST, $\Delta\theta_v$ and LCL for two legs crossing the front on day 49 are shown in Fig. 13. The cloud field was dominated by high level clouds with bases below $-20$°C on both sides of the front. The lower level clouds were also distributed quite evenly across the front with cloud bases near the top of the boundary layer. As discussed above, the boundary layer was 700 and 600 m deep on the cold and warm side of the front, respectively. The LCL was lower than on day 48 with heights ranging from about 400 to 700 m. This was due primarily to higher moisture contents in the boundary layer, although this effect was partially offset by higher temperatures. In the vicinity of the front there was a decrease in humidity and temperature which may have been due to local subsidence (Friehe and Luu, private communication). This resulted in the highest lifting condensation levels and fewer low level clouds immediately down wind of the front. The LCL heights were much lower on both sides of the front, so that even weak surface driven convection could be responsible for substantial cloudiness. On both sides of the front the LCL was below the top of the MABL, determined from the vertical profiles, within either the IBL on the cold side, or within the mixed layer on the warm side of the front.

The time series of $\theta$ indicates that warmer air has crossed the front with the sharpest gradients over the colder water approximately 20 km downwind of the front (the aircraft flew at about 100 m s$^{-1}$, thus 20 km $\equiv$ 3.5 min.). Estimates of $\Delta\theta_v$ (approx. $-1$°C) and the buoyancy flux, discussed here, on the cold side of the front indicate that there was little vertical exchange between the developing IBL and the overlying boundary layer. Thus the cloud field probably developed over the warmer water and was advected to the north of the front.

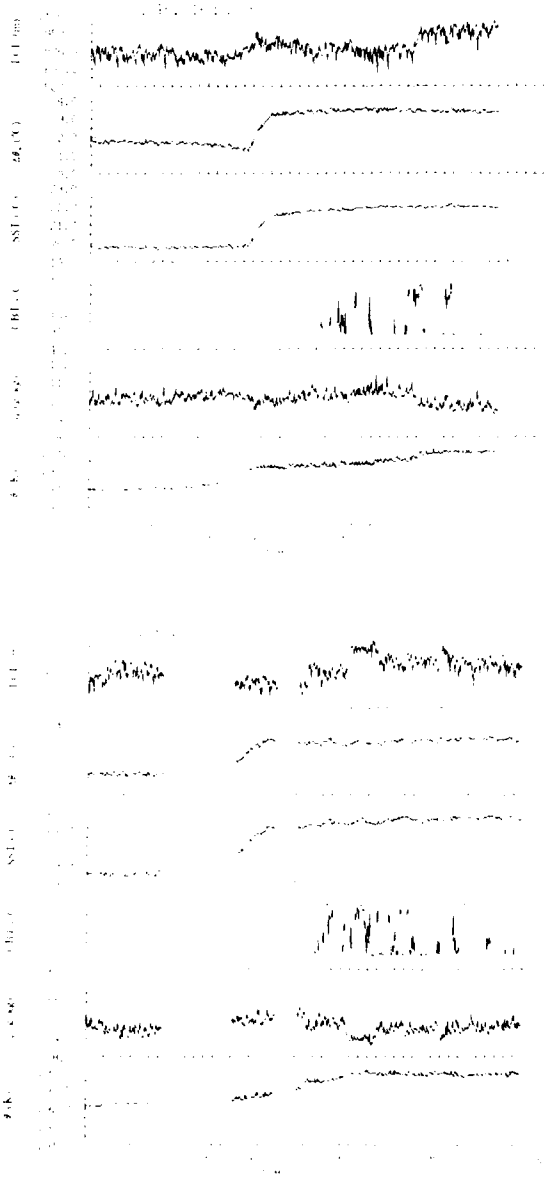

FIG. 12. Time series of $\theta$, $q$, CBT, SST, $\Delta\theta_v$ and LCL for two crossings of the front on day 48: (a) leg 2-3, (b) 5-6. A gap appears in the time series on the second leg due to a fault in data acquisition.

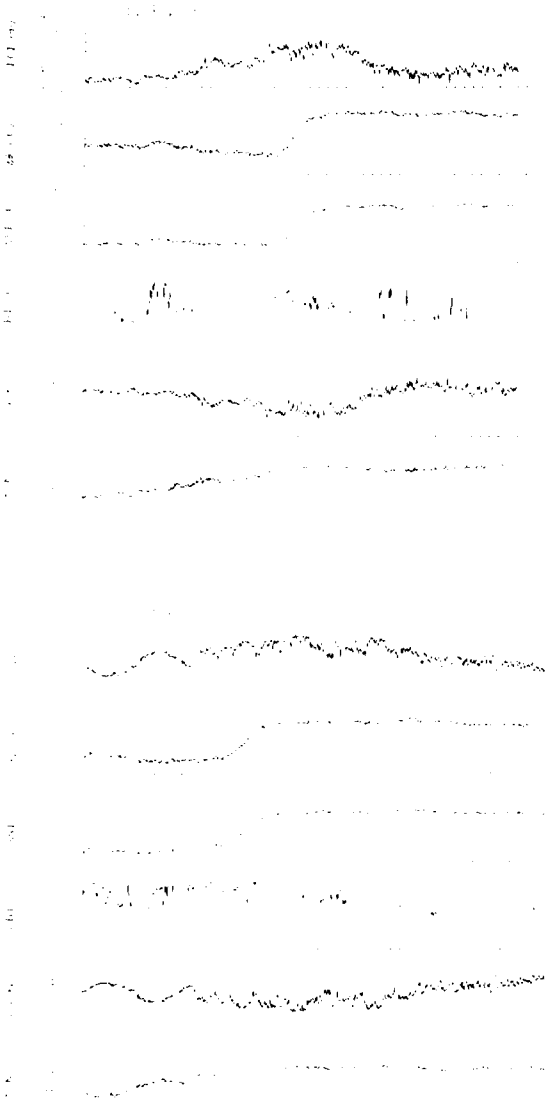

FIG. 13. As in Fig. 12, except for day 49.

The largest sea–air temperature differences were observed on day 52 with the transport of air from the cooler water to the warmer water (Fig. 14). This air was apparently buoyant on both sides of the front; although, cloud elements were confined to the lowest LCL regions. On leg 2-3, the minimum LCLs were observed in the vicinity of the front. Although the vertical profiles indicate that there was a shallow surface layer on the cold side of the front, the strongest coupling between the ocean and the atmosphere occurred under these conditions. These clouds appear to have developed within the mixed layer and, thus, may differ from those observed in the vertical profiles which had bases above 700 m. Visual observation indicated that these were shallow fair-weather cumulus cloud elements. Again the mixing ratio appears to be the dominant thermodynamic parameter.

An interesting feature of the atmospheric thermodynamic structure is the apparent sensitivity of the air over the cooler water to the warmer water downwind of the front. That is, although the flow is from the cooler side of the front to the warmer side the potential tem-

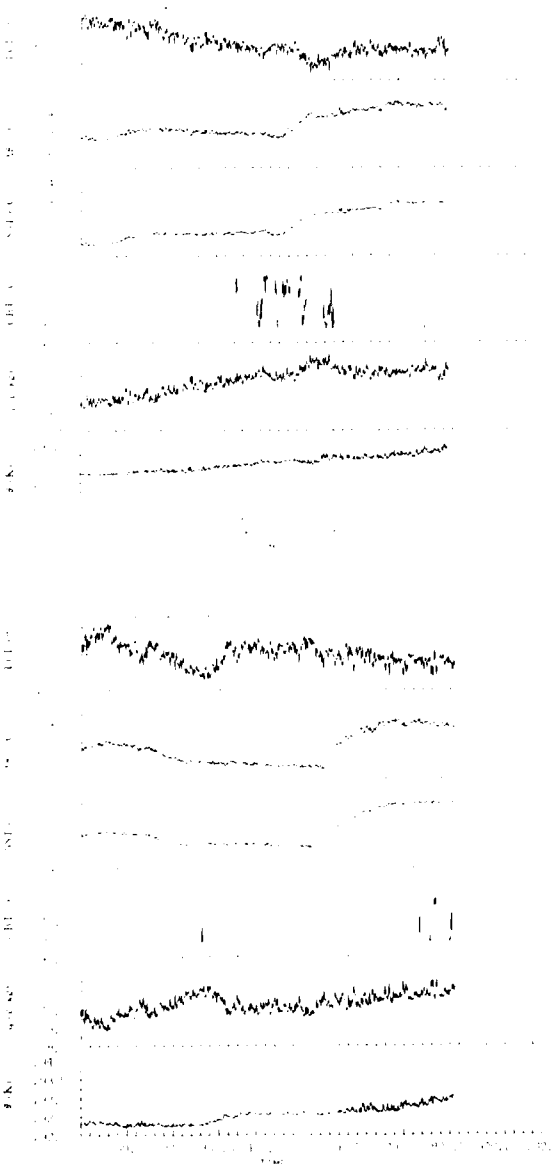

FIG. 14. As in Fig. 12, except for day 52.

perature and mixing ratio begin to increase before the air crosses the front. This is another indication of the possibility of secondary circulations in the vicinity of the front.

## 6. Turbulence structure

The development of the entire MABL is likely to depend strongly on variations in the turbulence structure in the vicinity of the front. This can be investigated using conditional sampling techniques. Recent studies of subcloud layer convection have used either amplitude threshold conditional sampling techniques (e.g., Holland 1973; Lenschow and Stephens 1980; Greenhut and Khalsa 1982, 1987; Khalsa and Greenhut 1985) or bivariate conditional sampling techniques (e.g., Wilczak and Businger 1983; Grossman 1984; Prabhu and Grossman 1985; Rogers and Businger 1988). In this study the bivariate method proposed by Holland (1973) is emphasized.

### a. *Conditional sampling techniques*

Conditional sampling techniques have been successfully employed to estimate turbulent fluxes of heat and moisture from noncontinuous time series of variances. Holland has shown that the vertical flux of a passive scaler, $\xi$, can be decomposed into four components using a bivariate conditional sampling technique. Thus,

$$\overline{w'\xi'} = \underset{(++)}{\overline{w'_+\xi'_+}} + \underset{(+-)}{\overline{w'_+\xi'_-}} + \underset{(--)}{\overline{w'_-\xi'_-}} + \underset{(-+)}{\overline{w'_-\xi'_+}}. \quad (1)$$

If $\xi'$ is replaced by $\theta'_v$, the fluctuating component of the virtual potential temperature, Eq. (1) represents the buoyancy flux. The dominant feature is a cell core associated with upward moving positively buoyant air (++) or downward moving negatively buoyant air (−−) which represents a direct flux (Fig. 15). A much smaller direct flux is associated with mass compensation flow as cells move upward or downward. Grossman (1984) suggests that, in this case, $w'$, the fluctuating component of the vertical velocity, is small while $\theta'_v$ is large. Small scale mixing (entrainment–detrainment) is identified as air moving laterally between cells. Air entrained into an upward moving cell or detrained from a downward moving cell is represented by $w'_-\theta v'_+$, while air detrained from an upward moving cell or entrained into a downward moving cell is given by $w'_+\theta v'_-$. In addition, entrainment occurring at the top of a cell and overshooting of parcels may also contribute to the indirect flux or negative flux (Wilczak and Businger 1983).

An indicator function is defined to produce four categories,

$$I(w' > 0, \theta'_v > 0) \equiv +2$$

$$I(w' > 0, \theta'_v < 0) \equiv +1$$

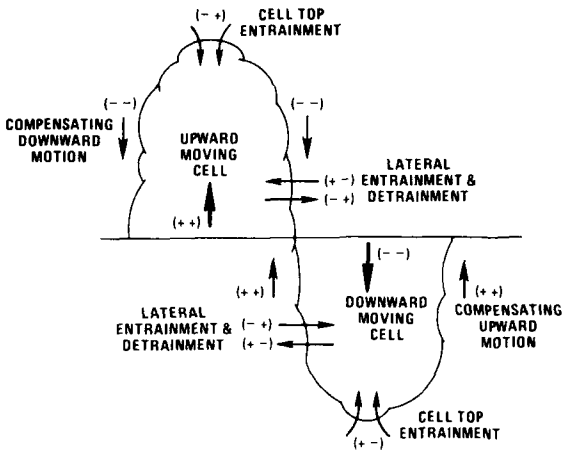


FIG. 15. Schematic of direct and indirect fluxes related to upward and downward moving cells.

$$I(w' < 0, \theta'_v > 0) \equiv -1$$

$$I(w' < 0, \theta'_v < 0) \equiv -2. \quad (2)$$

These indices are used to find discrete time intervals associated with the four categories over the length of the time series. Combinations involving zero have not been included because they are very rare.

Equation 2 can be modified to give indices based on the threshold conditional sampling technique of Khalsa and Greenhut (1985), so

$$I(w' \geq w'_{th+}, \theta v' > 0) \equiv +2$$

$$I(w' \geq w'_{th+}, \theta v' < 0) \equiv +1$$

$$I(w'_{th-} < w' < w'_{th+}) \equiv 0$$

$$I(w' \leq w'_{th-}, \theta v' > 0) \equiv -1$$

$$I(w' \leq w'_{th-}, \theta v' < 0) \equiv -2 \quad (3)$$

where $I \equiv 0$ represents the environment determined by the vertical velocity threshold, $w'_{th-}$. However, Khalsa and Greenhut (1985) consider only the velocity term so that (3) becomes

$$I(w' \geq w'_{th+}) \equiv +1$$

$$I(w'_{th-} < w' < w'_{th+}) \equiv 0$$

$$I(w' \leq w'_{th-}) \equiv -1 \quad (4)$$

In addition, Khalsa and Greenhut include the criterion that events must be at least 0.2 s in duration or about 22 m in length. The threshold for updrafts (downdrafts) $w'_{th+}$ ($w'_{th-}$) is set equal to the square root of one-half of the variance of the positive (negative) values of $w'$ about $w' = 0$ (Greenhut and Khalsa 1987). This approach tends to include what may be smaller scale mixing events, such as mixing into cell tops and local compensating flow, into the environment

category. Khalsa and Greenhut (1988) presented results from a study of NOAA P-3 aircraft data from FASINEX. This showed that the environment occupied about 70% of the total area and contributed between 22% and 29% of the buoyancy flux. It was assumed that all of the flux should be associated with well-defined cell areas. As pointed out by Grossman (1984) such obvious cell-like signatures are not always observed since aircraft of shipborne sensors do not always sample the most active part of a cell. However, if long enough time series are obtained in a random field of convective cells, statistics representative of a single convective cell will emerge (Frisch and Businger 1973).

### b. *Turbulence statistics*

Statistics on the mean partitioned fluxes for each day are estimated from two of the four frontal crossings flown on each circuit of the box pattern. Each leg is divided into three segments: warm, cold and the frontal region. The latter is loosely defined as the region containing the largest gradients of temperature and moisture. The MABL consisted of discrete cell-like structures with a substantial contribution to the buoyancy flux from smaller less coherent elements.

The fractional time and mean partitioned fluxes for day 48 are shown in Table 2. The direct fluxes accounted for an average of 62% of the total time with the remaining 38% in the indirect modes on the warmer side of the front, and 54% in the direct mode and 46% in the indirect mode on the cooler side of the front. The partitioned fluxes over the warm water can be compared with the estimates of Grossman (1984) of 64% and 36% in direct and indirect modes, respectively, over the Atlantic trade winds near Barbados. The ratio of updraft area to downdraft area was similar on both sides of the front (0.82 over the warmer water and 0.80 over the colder water). However, the partitioned fluxes indicate that direct convection and turbulent mixing were much more active over the warmer water than the cooler water with the frontal area acting as a transitional region on a scale of about 20 km (large fluxes are anticipated in the immediate vicinity of the front; however, the feature is too sharp to produce statistically significant results in this area). Furthermore, the updrafts were much more intense relative to the downdrafts on the warmer side of the front than on the cooler side. The field appears to have been divided between weakly descending regions and narrow more intense updrafts. Calculating the time spent in updrafts as a percentage of the total time spent in drafts reveals that 44% of the time was occupied by updrafts on both sides of the front. Mixing or indirect fluxes were a significant portion of the total flux. As observed by Grossman (1984) in the Atlantic trade winds near Barbados, the indirect fluxes were almost equally divided between the entrainment and detrainment modes.

On the warm side of the front on day 49, the direct flux accounted for 64% of the total time which was similar to the structure observed on day 48 (Table 3). However, downwind of this, on the cold side of the front the direct flux accounted for only 39% of the total time with the flux dominated by the indirect or mixing modes. The ratio of the updraft area to downdraft area was 0.84 on the warmer side and 1.07 on the cooler side of the front. Recalling Fig. 13, the virtual potential temperature of the air as it crossed from the warm to the cold side of the front was higher than the temperature of the underlying surface. Thus, as the air crossed the front, the surface-driven buoyancy flux was suppressed and turbulence within the surface layer began to collapse.

The buoyancy fluxes are much larger everywhere on day 52 than in the previous cases (Table 4). The dominance of the surface-driven turbulent mixing processes is observed in the direct fluxes which occupied about 64% of the total time. The ratio of updrafts to downdrafts varied from 0.75 on the warmer side to 0.77 on the cooler side of the front. The updrafts were much more intense than the downdrafts and both were substantially larger than the indirect fluxes. The updrafts over the warmer water were about 1.4 times larger than observed upwind over the colder water. Such strong surface forcing can clearly explain the absence of an IBL over the warmer water.

## 7. Discussion and concluding remarks

Ocean fronts, in the subtropical convergence zone, have surface temperature gradients of up to 0.4°C $km^{-1}$ which are relatively constant on time scales of at least a week and detectable as coherent structures for longer periods (Van Woert 1982). During FASINEX a quasi-stationary SST discontinuity of 2°C was maintained across the frontal zone throughout the measurement period. In this geographical area the atmospheric synoptic-scale forcing is generally relatively weak so that the response of the MABL to the front can be readily determined. The primary response of the atmosphere

TABLE 2. Mean partitioned buoyancy fluxes ($10^3$ K m $s^{-1}$) for day 48. The percentage area occupied by each partition is shown in parentheses. The fluxes are divided into three segments: over the warmer water, near the front, and over the colder water.

| Location | ++ | +− | −− | −+ | Total flux |
|---|---|---|---|---|---|
| Warmer water | 14.29 (28) | −2.74 (20) | 9.42 (34) | −3.53 (18) | 17.44 |
| Frontal region | 10.39 (26) | −3.49 (20) | 7.43 (31) | −4.17 (23) | 10.16 |
| Colder water | 4.89 (24) | −3.17 (23) | 3.81 (30) | −3.36 (23) | 2.17 |

TABLE 3. Mean partitioned buoyancy fluxes for day 49. (See Table 2 for complete explanation.)

| Location | ++ | +− | −− | −+ | Total flux |
|---|---|---|---|---|---|
| Warmer water | 7.37 (29) | −1.46 (18) | 4.92 (35) | 1.95 (18) | 8.88 |
| Frontal region | 2.10 (20) | −2.97 (26) | 2.05 (24) | 2.63 (30) | 1.45 |
| Colder water | 2.40 (20) | −6.18 (33) | 2.33 (19) | 8.59 (28) | 9.99 |

to changes in the SST occurred in the surface-related turbulent fluxes. These provide the heat, moisture and momentum which control the initial development of MABL clouds. These are the "forced" clouds described by Stull (1985) and Rogers et al. (1985). This cloud type depends on a continuous input of heat and moisture. Above the level of free convection (LFC) these clouds become a so-called "active," independent cloud fraction which no longer depends directly on the surface forcing (Stull 1985). The present observations suggest another category where "forced" clouds are disconnected from the direct thermal forcing by the development of either a surface layer or a transition layer below cloud base. These clouds and the surrounding structure are maintained primarily by turbulence mixing generated within the cloud layer. As pointed out by Rogers et al. (1985) an obvious source of turbulent kinetic energy within the cloud field is radiative warming at cloud base. Other observations indicate that short wave heating of the upper part of the cloud layer coupled with cloud-top radiative cooling strongly maintains kinetic energy production in the upper part of a cloud, but leads to the decoupling of the cloud and subcloud layers (Nicholls and Leighton 1986; Boers and Betts 1988). This mechanism maintains turbulent mixing within the cloud, but diminishes it in the upper part of the subcloud layer. These clouds may be referred to as "radiatively forced" ($R_f$) rather than "thermally forced" ($R_t$). Thus, although clouds are initiated by thermal forcing, the continuity of the field over the ocean depends to a large extent on mixing induced by turbulence generated within the cloud layer. This could account for the longevity of the rather tenuous, but extensive, thin layers of cloud which were frequently observed during FASINEX. A cloud-capped well-mixed layer can be maintained if the cloud layer is not eroded due to entrainment. In this case, the extension of the turbulence generated within the cloud layer below cloud base can also be important in controlling boundary layer ventilation. However, previous results have shown that, if cloud-top entrainment instability develops, mixing through cloud top and cloud base can account for the development of a dry stable layer between cloud base and the top of the mixed layer (Nicholls 1984; Rogers 1986). The vertical exchange of heat and moisture between the subcloud layer and the cloud layer is limited, and the cloud layer erodes from the base up through the influx of large amounts of dry air from aloft (Rogers 1986).

An important feature of the FASINEX boundary layer was the presence of an internal boundary layer over the colder water. The development of an IBL depends primarily on changes in the surface-related fluxes. The observations indicate that this layer was most pronounced over the cold water when the air flowed from the warm side of the front. This was generally the case on both day 48 and 49. Vertical exchange between the surface and the overlying boundary layer on the warm side of the front was not restricted. Here, the IBL was absent so that the entire boundary layer was strongly coupled to the surface fluxes. The IBL is assumed to be forced primarily by surface-driven mixing processes; therefore, the depth of the layer should scale with a surface parameter. It has been shown previously (Nicholls et al. 1983) that in weakly turbulent regions the mixed layer can be scaled using the friction velocity, $u_*$, and the Coriolis parameter, $f$, rather than the depth of the entire convective boundary layer. Nicholls et al. (1983) observed that the JASIN mixed layer depth, $h$, was approximately proportional to $u_*/f$, which is a prediction of the neutral Ekman layer similarity theory with a constant of proportionality of about 0.2. Nicholls and Leighton (1986) presented results from marine boundary layer measurements around the United Kingdom. On several occasions a well-developed surface of Ekman layer was present while, at other times, the mixed layer extended down to the sea surface. The constant of proportionality varied from 0.18 to 0.13 for these two MABL types, respectively. On FASINEX day 49, the IBL was between 200 and 350 m deep on the cold side of the front. On the warm side of the front the mixed layer extended

TABLE 4. Mean partitioned buoyancy fluxes for day 52. (See Table 2 for a complete explanation.)

| Location | ++ | +− | −− | −+ | Total flux |
|---|---|---|---|---|---|
| Warmer water | 15.18 (29) | −2.42 (17) | 8.97 (38) | −2.53 (16) | 19.20 |
| Frontal region | 9.51 (27) | −1.87 (18) | 5.91 (36) | −2.27 (19) | 11.28 |
| Colder water | 10.62 (28) | −2.07 (17) | 6.85 (37) | −2.61 (18) | 12.79 |

down to the surface and up to about 500 m altitude. Friehe and Luu (personal communication) estimate $u_*^2$ to be 0.06 and 0.12 $m^2 s^{-2}$ on the cold and warm sides of the front, respectively. Using these values the constant of proportionality is approximately 0.2 on the warm side of the front and between 0.1 and 0.2 on the cold side of the front (Table 5). The weaker fluxes on the cold side lead to the development of a shallow IBL, rather than a well-mixed layer as the air moved across the front. The evolution of the overall MABL structure is strongly dependent on the stress which controls the depth of the IBL. The ability of this layer to support shear between the surface and the base of the mixed layer has important implications for the development of the cloud field and the extent to which the clouds are directly coupled to the surface forcing.

Clearly, on day 48 the clouds on the warm side of the front were organized in bands parallel to the wind and consequently strongly coupled to the surface. Over the colder water an IBL was observed and no clouds were encountered. On day 49 the boundary layer was strongly coupled to the surface forcing over the warmer water; although there was no evidence of organized convection, the cloud capped mixed layer consisted of about 80% air that originated locally near the ocean surface. Over the colder water a well-defined IBL and weak surface forcing suggest that there is negligible coupling between the surface and the cloud field. In this case the cloud layer consisted of about 50% air originating near the ocean surface at a higher SST than observed in the immediate vicinity of the measurements. In this case the cloud field and the mixed layer were most likely maintained by radiatively driven turbulence mixing processes. The higher fraction of surface air in the mixed layer and lower buoyancy flux over the warmer water on day 49 compared with day 48 suggests that on day 49 the air has been in contact with a nearly constant SST for some time. The cloud layer will be connected to the surface although the buoyancy flux will weaken as more moisture is input to the lower atmosphere.

On day 52, with the wind blowing from over the cold water to the warm water, banded clouds parallel to the surface wind were observed in the satellite image on both sides of the front. In situ measurements indicate that the cloud elements were limited to regions of high mixing ratio and low LCL. The cloud fields varied from day to day; however, the $R_r$ fraction on both sides of the front appears to have originated over the warmer water. Thus, the cloud field and mixed layer observed on the cold side of the front on days 48 and 49 were probably advected from warmer water.

TABLE 5. Mixed layer and surface layer scaling for day 49.

| Parameter | Warmer water | Colder water |
|---|---|---|
| $u_*^2$ ($m^2 s^{-2}$) | 0.12 | 0.06 |
| $u_*/f$ (m) | 2483.6 | 1756.2 |
| $h$ (m) | 500.0 | 200.0 |
| $fh/u_*$ | .201 | 0.114 |

The origin of this rather distinctive "multiple boundary layer structure" is of particular interest since the superposition of an elevated cloud layer affects the development of the underlying MABL. As already discussed, if the elevated cloud/mixed layer structure is maintained by convection driven by cloud top radiative cooling, continuity of the field over considerable distances would be expected. Nearly continuous cloud bands were observed over several hundred kilometers from the satellite images during FASINEX. This suggests that the upper level mixed layers had a distant origin, and were advected across the top of the in situ boundary layer. The high moisture contents observed in the elevated layers on days 48 and 49, and the apparent equilibrium with warmer water suggests that this air could have originated in the upper level outflow of a deep convective cloud system to the south of the FASINEX area or, perhaps, even in the vicinity of the Gulf Stream.

The overall impact of this air on the developing MABL can only be speculated on at present; however, there is no evidence of strong vertical mixing between the elevated layers and the lower boundary layer. The maintenance of the cloud-capped boundary layer depends on cloud top entrainment, radiative transfer, cloud microphysics and surface-related processes (Rogers and Telford 1986). In the presence of two well mixed cloud layers, entrainment and radiative transfer through the top of the lower layer will be reduced because of the additional liquid water and vapor content associated with the air immediately above the MABL. In the absence of entrainment the MABL would have higher mixing ratios and lower temperatures which, in turn, could lead to forced cloud development in the lower part of the boundary layer.

Another important consideration is the rate at which the MABL approaches equilibrium with surface-forcing. The development of an IBL due to the advection of warm air over a sharp SST discontinuity to cool water instantly changes the lower boundary conditions. These restrict the exchange of heat, moisture and momentum between the surface and the upper part of the MABL. Given a sufficient, but as yet unknown, amount of time the boundary layer will adjust to the new surface forcing by redistributing heat and moisture throughout the MABL. Nicholls et al. (1982) suggest that the turbulence fluxes will adjust on a time scale of about $10^3$ s and the mean properties will adjust on a time scale of the order of a day. The uncertainty in this study is in the magnitude of the radiatively driven mixing processes which may control the exchange between the IBL and the upper parts of the boundary layer. If cloud top cooling is a significant process then this may lead to the complete overturning of the layer and the establishment of a MABL in equilibrium with the underlying

surface. Alternatively, if the cloud and subcloud layers are decoupled due to solar heating of the cloud layer then the IBL may erode upwards to form a new MABL without overturning the lower atmosphere. This could also result in the observed multiple mixed layer structures. Cool, moist air is transferred into the surface layer by the buoyancy flux forming a new MABL. Maintenance of this structure independently of the overlying air depends primarily on there being only weak turbulence in the upper part of the original mixed layer. These layers may be eroded only if there is an increase in either the surface fluxes or radiation-driven mixing in the overlying cloud layer. The conditional sampling statistics for day 49 reveal the early formation of the IBL close to the front. Turbulence near the surface collapses with the dissipation of organized convective elements through entrainment of the surrounding air into the convective parcels, or detrainment from the parcels to the environment. As discussed above, mixing in the upper part of the MABL continues unimpeded. The surface layer grows in response to the strong shear in this layer so that mechanical turbulence is effectively redistributing the cool, moist air originating at the surface.

These observations suggest that surface-forced clouds originated mostly over the warmer water and interaction between the surface and the upper part of the MABL is limited by the presence of an internal boundary layer over the cold water. In contrast, Gautier and Bates (1988) observed that, on a monthly time scale, the largest cloud fraction occurred over the colder water to the north of the region. This suggests that ocean fronts may have a significantly different effect on MABL cloud development on relatively short time scales compared with the longer term processes. This is consistent with the expectation that the mean boundary layer adjustment takes place on a time scale of the order of a day. Thus, once the MABL has returned to equilibrium with the surface, weak convection can produce extensive regions of low cloud over the cooler water.

In conclusion, the primary effect of the front is on the surface stress and buoyancy flux, which can lead to the development of an internal boundary layer. This exerts a significant control on the evolution of the entire cloud-capped MABL which, in turn, may lead to the formation of a complex boundary layer structure.

*Acknowledgments.* The author gratefully acknowledges the crew of NCAR Electra aircraft and colleagues who made the FASINEX study possible. Special thanks to Joost Businger, Carl Friehe, Steve Stage and Bob Weller.

This work was funded in part by the Office of Naval Research under Contract USN N00014-88K-0474 and by the National Science Foundation through Grant ATM-8896168.

## REFERENCES

Betts, A. J., 1982: Saturation point analysis of moist convective overturning. *J. Atmos. Sci.*, **39**, 1484–1505.

———, and B. A. Albrecht, 1987: Conserved variable analysis of the convective boundary layer thermodynamic structure over the tropical oceans. *J. Atmos. Sci.*, **44**, 83–99.

Boers, R., and A. K. Betts, 1988: Saturation point structure of marine stratocumulus clouds. *J. Atmos. Sci.*, **45**, 1156–1175.

Businger, J. A., and W. J. Shaw, 1984: The response of the marine boundary layer to mesoscale variations in sea surface temperature. *Dyn. Atmos. Oceans*, **8**, 267–281.

Charlson, R. J., J. E. Lovelock, M. O. Andreae and S. G. Warren, 1987: Oceanic phytoplankton, atmospheric sulfur, cloud albedo and climate. *Nature*, **326**, 655–661.

Deardorff, J. W., 1980: Cloud top entrainment instability. *J. Atmos. Sci.*, **37**, 131–147.

Friehe, C. A., and E. R. Williams, 1988: Aircraft measurements in FASINEX. Preprints, *Seventh Conf. on Ocean–Atmosphere Interaction*, Anaheim, CA. Amer. Meteor. Soc., 38–40.

Frisch, A. S., and J. A. Businger, 1973: A study of convective elements in the atmospheric surface layer. *Bound.-Layer Meteor.*, **3**, 301–328.

Gardiner, B. A., and D. P. Rogers, 1987: On mixing in continental cumulus clouds. *J. Atmos. Sci.*, **44**, 250–259.

Gautier, C., and J. Bates, 1988: Influence of an ocean thermal front on cloud characteristics during FASINEX. Preprints, *Seventh Conf. on Ocean–Atmosphere Interaction*, Anaheim, CA. Amer. Meteor. Soc., 194–198.

Greenhut, G. K., and S. J. S. Khalsa, 1982: Updraft and downdraft events in the atmospheric boundary layer over the equatorial Pacific Ocean. *J. Atmos. Sci.*, **39**, 1803–1818.

———, and ———, 1987: Convective elements in the marine atmospheric boundary layer. Part I: Conditional sampling statistics. *J. Climate Appl. Meteor.*, **26**, 813–822.

Grossman, R. L., 1984: Bivariate conditional sampling of moisture flux over a tropical ocean. *J. Atmos. Sci.*, **41**, 3228–3253.

Guymer, T. H., J. A. Businger, K. B. Katsaros, W. J. Shaw, P. K. Taylor, W. G. Large and R. J. Payne, 1983: Transfer processes at the air-sea interface. *Phil. Trans. Roy. Soc. London*, **308**, 253–273.

Halliwell, V. M., E. Bohm and P. Cornillon, 1987: Ship-, satellite- and air-derived sea surface temperature fronts for FASINEX. Graduate School of Oceanography, University of Rhode Island, Narragansett, RI. Tech. Rep., 87-4, FASINEX Tech. Rep. #41, 115 pp.

Holland, J. Z., 1973: A statistical method for analyzing wave shapes and phase relationships of fluctuating geophysical variables. *J. Phys. Oceanogr.*, **3**, 139–155.

Khalsa, S. J. S., and G. K. Greenhut, 1985: Conditional sampling of updrafts and downdrafts in the marine atmospheric boundary layer. *J. Atmos. Sci.*, **42**, 2550–2562.

———, and ———, 1988: Surface forcing and turbulence structure in the marine atmospheric boundary layer during FASINEX. Preprints, *Seventh Conf. on Ocean–Atmosphere Interaction*, Anaheim, CA. Amer. Meteor. Soc., 64–67.

Kraus, E. B., and L. D. Leslie, 1982: The interactive evolution of the oceanic and atmospheric boundary layers in the source regions of the trades. *J. Atmos. Sci.*, **39**, 2760–2772.

Lenschow, D. H., 1986: Aircraft measurements in the boundary layer. *Probing the Atmospheric Boundary Layer*, D. H. Lenschow, Ed., Amer. Meteor. Soc., 39–56.

———, and P. L. Stephens, 1980: The role of thermals in the convective boundary layer. *Bound.-Layer Meteor.*, **19**, 509–532.

Mahrt, L., and J. Paumier, 1982: Cloud top entrainment instability observed in AMTEX. *J. Atmos. Sci.*, **39**, 622–634.

Manabe, S., and R. T. Wetherald, 1967: Thermal equilibrium of the atmosphere with a given distribution of relative humidity. *J. Atmos. Sci.*, **24**, 241–259.

Nicholls, S., 1984: The dynamics of stratocumulus: aircraft observations and comparisons with a mixed-layer model. *Quart. J. Roy. Meteor. Soc.*, **110**, 783–820.

——, and M. A. LeMone, 1980: The fair weather boundary layer in GATE: The relationship of subcloud fluxes and structure to the distribution and enhancement of cumulus cloud. *J. Atmos. Sci.*, **37**, 2051–2067.

——, and J. Leighton, 1986: An observational study of the structure of stratiform cloud sheets. Part I: Structure. *Quart. J. Roy. Meteor. Soc.*, **112**, 431–460.

——, M. A. LeMone and G. Sommeria, 1982: The simulation of a fair weather marine boundary layer in GATE using a three-dimensional model. *Quart. J. Roy. Meteor. Soc.*, **108**, 167–190.

——, B. Brümmer, F. Fiedler, A. Grant, T. Hauf, G. Jenkins, C. Readings and W. Shaw, 1983: The structure of the turbulent atmospheric boundary layer. *Phil. Trans. Roy. Soc. Lond.*, **308A**, 221–230.

Paluch, I. R., 1979: The entrainment mechanism of Colorado cumuli. *J. Atmos. Sci.*, **36**, 2467–2478.

Pollard, R. T., 1978: The joint air–sea interaction experiment—JASIN 1978. *Bull. Amer. Meteor. Soc.*, **59**, 1310–1318.

——, 1986: Frontal surveys with a towed profiling conductivity/temperature/depth measurement package (SeaSor). *Nature*, **32**, 433–435.

Prabhu, A., and R. L. Grossman, 1985: The turbulent humidity flux budget in the central Arabian Sea subcloud layer during the summer monsoon. *Proc. Seventh Symp. on Turbulence and Diffusion*, Boulder, CO, Amer. Meteor. Soc., 71–77.

Rogers, D. P., 1986: On the onset of entrainment instability over the ocean. *Bound.-Layer Meteor.*, **37**, 167–182.

——, and J. W. Telford, 1986: Metastable stratus tops. *Quart. J. Roy. Meteor. Soc.*, **112**, 481–500.

——, and J. A. Businger, 1988: The influence of a sea surface temperature discontinuity on the structure of the atmospheric boundary layer. Preprints, *Seventh Conf. on Ocean–Atmosphere Interaction*, Anaheim, CA, Amer. Meteor. Soc., 60–63.

——, —— and H. Charnock, 1985: A numerical investigation of the JASIN atmospheric boundary layer. *Bound.-Layer Meteor.*, **32**, 373–399.

Schneider, S. H., W. M. Washington and R. M. Chervin, 1978: Cloudiness as a climate feedback mechanism: effects on cloud amounts of prescribed global and regional surface temperature changes in the NCAR GCM. *J. Atmos. Sci.*, **35**, 2207–2221.

Shukla, J., and Y. Sud, 1981: Effect of cloud-radiation feedback on the climate of a general circulation model. *J. Atmos. Sci.*, **38**, 2337–2353.

Stage, S. A., and R. A. Weller, 1985: The frontal air–sea interaction experiment (FASINEX). Part I: Background and scientific objectives. *Bull. Amer. Meteor. Soc.*, **66**, 1511–1520.

——, and ——, 1986: The frontal air–sea interaction experiment (FASINEX). Part II: Experimental plan. *Bull. Amer. Meteor. Soc.*, **67**, 1511–1520.

Stull, R. B., 1985: A fair-weather cumulus cloud classification scheme for mixed layer studies. *J. Climate Appl. Meteor.*, **24**, 49–56.

Taylor, G. I., 1917: The formation of fog and mist. *Quart. J. Roy. Meteor. Soc.*, **43**, 241–268.

Van Woert, M., 1982: The subtropical front: satellite observations during FRONTS 80. *J. Geophys. Res.*, **87**, 9523–9536.

Wilczak, J. M., and J. A. Businger, 1983: Thermally indirect motions in the convective atmospheric boundary layer. *J. Atmos. Sci.*, **40**, 343–358.